Mon. Not. R. Astron. Soc. **331,** 369–375 (2002)

The properties of the X-ray holes in the intracluster medium of the Perseus cluster

A. C. Fabian,[1★] A. Celotti,[2] K. M. Blundell,[3] N. E. Kassim[4] and R. A. Perley[5]

[1]*Institute of Astronomy, Madingley Road, Cambridge CB3 0HA*
[2]*SISSA, via Beirut 2-4, 34014 Trieste, Italy*
[3]*Department of Astrophysics, Keble Road, Oxford OX1 3RH*
[4]*NRL, Code 7213, Washington DC 20375-5351, USA*
[5]*NRAO, PO Box 0, Socorro, NM 87801-0387, USA*

Accepted 2001 November 20. Received 2001 August 2

ABSTRACT

High-resolution X-ray and low-frequency radio imaging now allow us to examine in detail the interaction and physical properties of the radio source 3C 84 and the surrounding thermal gas. The radiative and dynamical properties of the inner X-ray holes, which coincide with the radio lobes, indicate that the ratio of the energy factor k to the filling factor f is in the range $180 < k/f < 500$. We define k to be the ratio of the total particle energy to that of the electrons radiating above a fiducial frequency of 10 MHz. The relativistic plasma and magnetic field are not in equipartition, since the field must be a factor of 4 or more lower than required for pressure balance. Unexpected steep-spectrum spurs in the low-frequency radio maps point to outer X-ray holes, which are plausibly buoyant old radio lobes. The evidence that the inner lobes are currently expanding subsonically, yet have not detached due to buoyancy, and the requirement that the synchrotron cooling time must exceed the age of the hole enable us to constrain the jet power of the nucleus to between 10^{44} and 10^{45} erg s^{-1}, depending on the filling factor of the relativistic plasma.

Key words: galaxies: clusters: individual: Perseus – cooling flows – galaxies: individual: NGC 1275 – X-rays: galaxies.

1 INTRODUCTION

The Perseus cluster of galaxies, A 426, at a redshift $z = 0.0183$ is the brightest cluster X-ray source in the sky. The X-ray surface brightness peaks around the radio source 3C 84 in the central galaxy NGC 1275. The inner radio lobes of 3C 84 clearly interact with the X-ray-emitting intracluster gas, leading to X-ray holes north and south of the nucleus (Böhringer et al. 1993; Churazov et al. 2000; Fabian et al. 2000; fig. 1). Outer holes are also seen (Fabian et al. 2000) which do not correspond to any structures on high-frequency (∼GHz) radio maps. Here we investigate the properties of the inner and outer X-ray holes and show that the outer holes lie at the ends of spurs of low-frequency radio emission seen at 74 MHz.

A comparison of the *ROSAT* High Resolution Imager data (Böhringer et al. 1993) with 1.4 GHz radio data (Pedlar et al. 1990) showed that equipartition radio plasma was probably underpressured with respect to the surrounding thermal intracluster medium. With the present *Chandra* data (Fabian et al. 2000) we now have temperature information on the scale of the holes and can estimate the thermal pressure much better. We find that the radio plasma and the intracluster gas can only be in pressure equilibrium if the magnetic field has a pressure much lower than required for equipartition.

The combination of X-ray and radio data allows improved estimates to be made of the total energy released by the radio source, and of k, the factor that accounts for the energy carried by the particles in the radio plasma in addition to that of the electrons radiating above a fiducial level of 10 MHz. In Section 2 we present the data, and in Section 3 deduce the pressure within the radio lobes from standard equipartition arguments. We find a pressure mismatch with the surrounding thermal gas unless k/f is large. Then, assuming pressure equilibrium and a synchrotron lifetime argument, we show that the field is below equipartition. Using dynamical constraints we then deduce the power needed to supply the lobes. The outer lobes are discussed in Section 4. Our conclusions are reported in Section 5.

2 THE X-RAY AND RADIO DATA

The *Chandra* X-ray data have been presented by Fabian et al. (2000). Three separate exposures were made of the Perseus cluster:

★E-mail: acf@ast.cam.ac.uk

in 1999 for 10 ks with ACIS-I; on 2000 January 10 for 10 ks with ACIS-S; and on 2000 January 30 for 25 ks with ACIS-S. A study of the combined, cleaned data from the last two ACIS-S images, totalling 23.9 ks, will be presented by Schmidt et al. (2002); here we show an adaptively smoothed version of this last image as the top panel of Fig. 1, and a Gaussian-smoothed image from the ACIS-I data covering the band 0.6–3 keV as the lower panel. A 2–7 keV image from ACIS-S is shown in Fig. 2. The adaptively smoothed combined ACIS-S image is also used as the background to the contours in Figs 3 and 4.

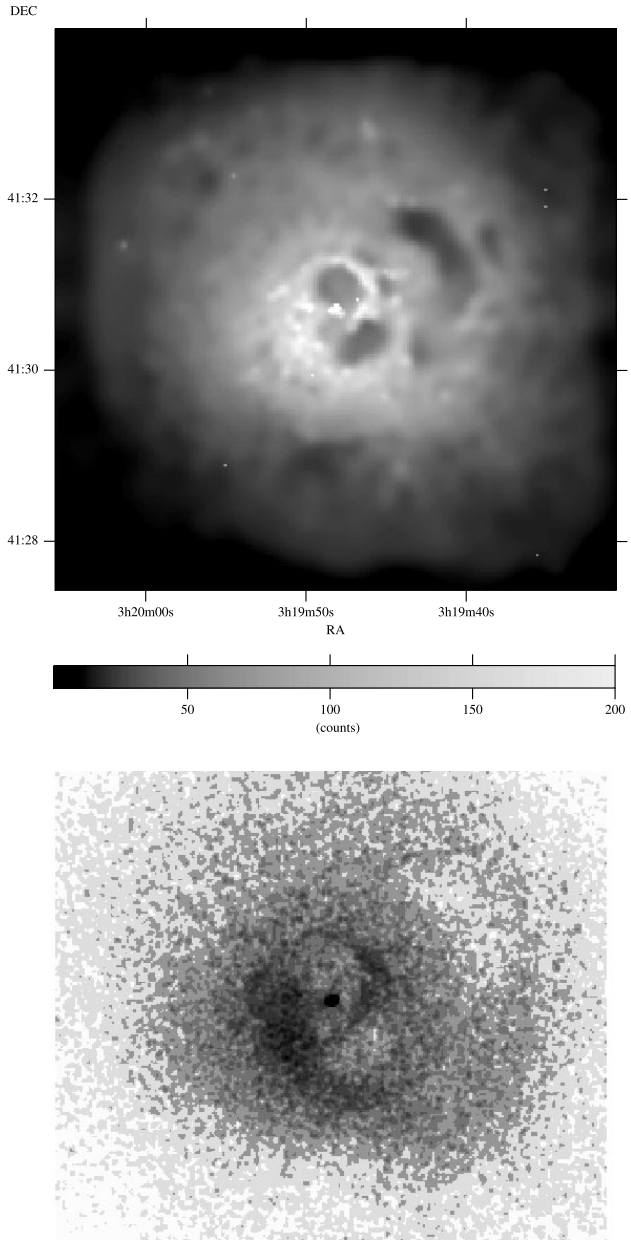

Figure 1. Top panel: combined, cleaned 23.9-ks ACIS-S X-ray image, using 2-arcsec bins and adaptively smoothed to a level corresponding to 3σ, showing the main features studied here. The two inner X-ray holes above and below the nucleus coincide with the main radio lobes of 3C 84, as seen at 1.4 GHz (Fig. 3, top). The large outer X-ray hole lies to the NW and another one is found to the S. Other smaller holes at larger radii from the nucleus are also seen but their significance is unclear. The colour bar has been truncated at 200 count per 4 square-arcsec pixel: the nucleus peaks at 911 count pixel^{-1} (23.9 ks)$^{-1}$. Lower panel: ACIS-I image of the central 5-arcmin diameter region. Gaussian smoothing has been applied. This image shows the complex structure of the inner part better than the deeper ACIS-S images in Fabian et al. (2000; see also Fig. 2), since a stripe due to differing readout nodes is absent. The precise nature of the structures is not clear. The holes may be roughly in the plane of the sky, or possibly arranged in a more perpendicular sense with the apparent 'e' shape being part of a helix oriented partly along our line of sight.

The two inner holes, which we term the N and S lobes, are clearly seen, as is at least one outer hole to the NW (Figs 1 and 5; also seen in Einstein Observatory images; Fabian et al. 1981). A new hole is also seen about 1 arcmin S of the nucleus (Fabian et al. 2000; see lower panel in Fig. 3). The inner holes have sharp bright rims in soft X-ray maps and contain the X-ray-coolest gas in the images ($kT \sim 3$ keV; Fabian et al. 2000) so the rims are not due to shocks. No additional hard X-ray structures are seen in the 2–7 keV image (Fig. 2).

Note that, if the rims were due to strong shocks, the observed emissivity, which is proportional to $n^2 T^{-0.5}$ where n and T are the gas density and temperature, respectively, would change by a factor of $16(T_{\rm sh}/T_0)^{-0.5}$. The ratio of the temperature of the shocked to unshocked gas, $T_{\rm sh}/T_0$, is most unlikely to be so high that the shocked gas is not readily detectable.

The present data are inadequate to determine clearly whether the holes are real, i.e. devoid of any thermal gas, or apparent, i.e. partially filled with hot gas at the cluster virial temperature of about 7 keV. At constant pressure the X-ray emissivity varies as the inverse square of the gas temperature, so deep soft X-ray holes can be made by a factor of 2 difference in temperature.

The three-dimensional geometry of the holes is unclear. A simple picture is that the jets (see Pedlar et al. 1990) are close to the plane of the sky and that the holes are spherical. It is however, possible that the jets and alignment of the lobes are more along our line of sight; for example the S radio jet may contribute to the N hole. Note from Fig. 2 that the S continuation of the NW rim avoids the nucleus. We adopt a spherical geometry for the N hole in our calculations.

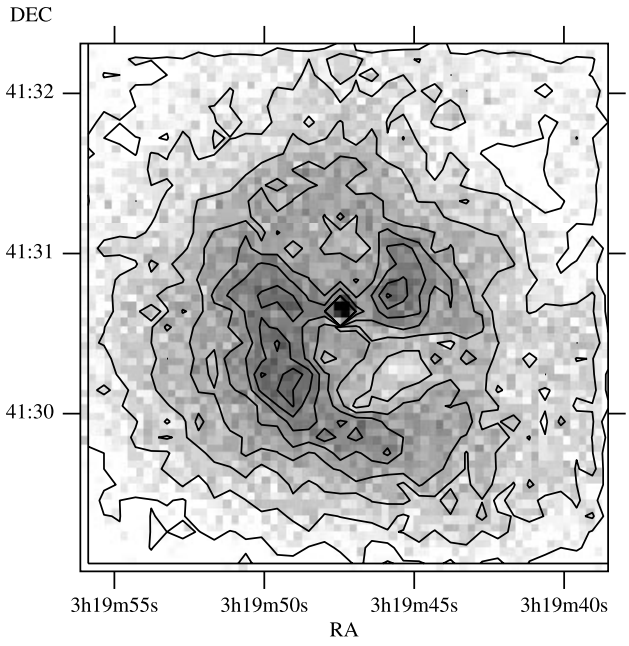

Figure 2. ACIS-S image (coordinates J2000) in the 2–7 keV band. The contour levels increase in steps of 10 count per 3 arcmin pixel from a lower level of 30. The inner holes therefore have 40–50 count pixel^{-1}.

The data have been deprojected (Fabian et al. 1981) to obtain the gas pressure profile up to the rims around the inner X-ray holes. This has confirmed that the simple (electron) pressure map shown in Fabian et al. (2000) is accurate to within 20 per cent. In particular, the total thermal pressure of the gas in the rim of the N radio lobe is $\sim 0.5\,\mathrm{keV\,cm^{-3}}$, reducing by a factor of 2 at the position of the outer NW lobe.

3C 84 was observed on 1998 March 7 simultaneously at 74 and 330 MHz using all 27 antennas of the VLA in its A-configuration. The data were observed in spectral line mode with 32 channels at 74 MHz and 64 channels at 330 MHz: this facilitates RFI excision (which is largely narrow-band) and helps to avoid bandwidth smearing. The on-source time was 64 min, which was spread

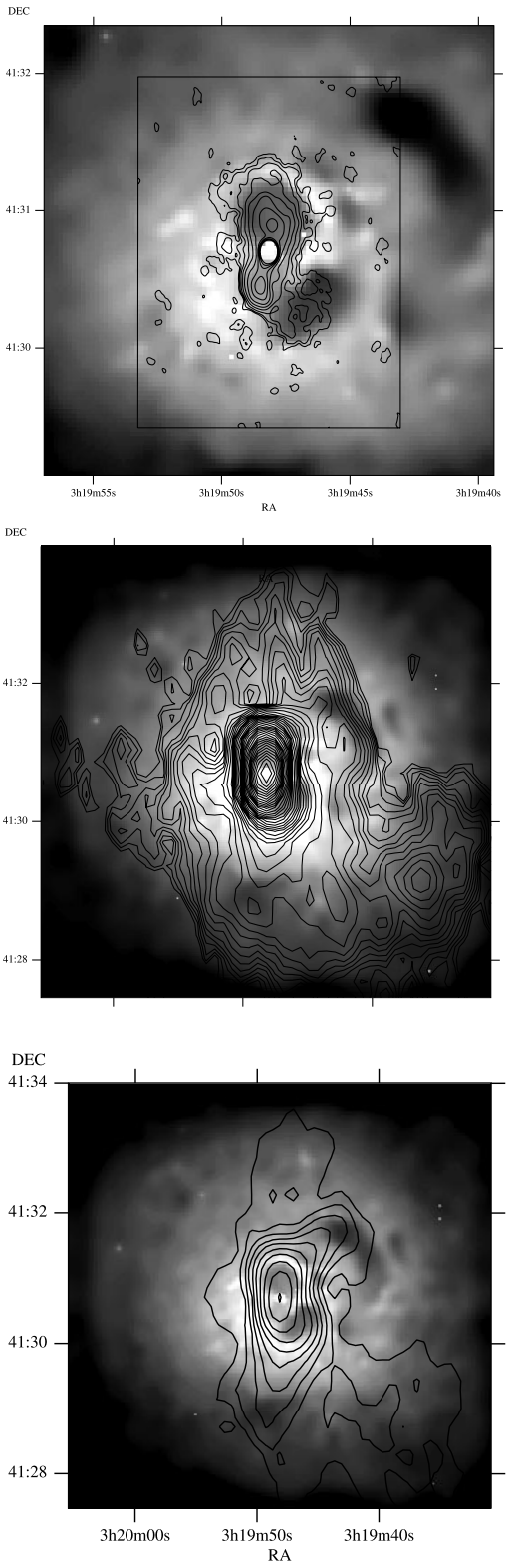

Figure 3. 1.4-GHz, 330-MHz and 74-MHz images of 3C 84 overlaid on the *Chandra* image of the core of the Perseus cluster. Note that the lower two images are on a smaller scale than the upper one.

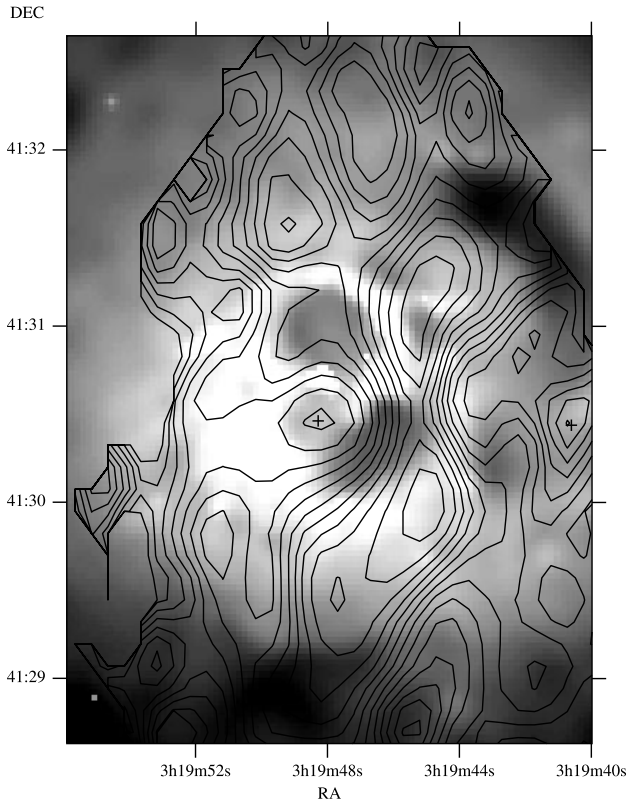

Figure 4. Spectral index map.'+' indicate regions of high spectral index, −0.7. The contours are in steps of 0.1 and go down to −1.7.

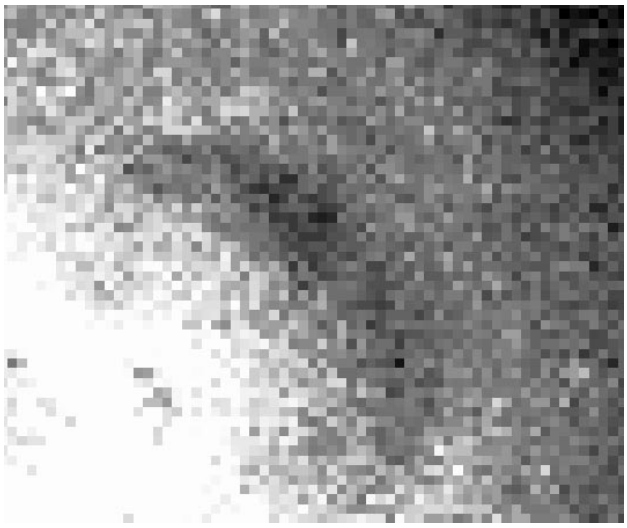

Figure 5. 0.5–7 keV, 100-arcsec high *Chandra* image of the outer NW hole. The mean count rate in the bottom of the hole is about one-half to one-third of that immediately to the SE.

throughout a 6-h period to maximize hour-angle coverage. Bandpass, amplitude and initial phase calibration are derived from several short scans of Cygnus A made throughout the observing run. Phase calibration utilized successive loops of self-calibration initiated with point-source models at both frequencies. This was possible because 3C 84 has enough short-spacing flux for self-calibration to work in its most elementary form and permit good phase solutions on time averages much shorter than the ionospheric incoherence time.

We show the 1.4-GHz (from G. Taylor, see Fabian et al. 2000), 330-MHz and 74-MHz radio maps overlaid on an adaptively smoothed X-ray image in Fig. 3. The spurs of the 74 MHz radio emission running NW and SSE both end at outer holes seen in the X-ray image (see also Fig. 5). The 74-MHz emission probably maps the regions containing the oldest relativistic electrons, plausibly indicating that the outer X-ray holes are old radio lobes, within which the most energetic electrons have lost their energy to synchrotron emission.

3 THE INNER RADIO LOBES

3.1 Equipartition between relativistic particles and magnetic field

We now apply standard synchrotron radiation theory to the inner lobes, in order to quantify the properties of the relativistic (particles and field) component. In particular we use region '3' of Pedlar et al. (1990), which is the brightest region of the N inner lobe (see top panel in Fig. 3).

The total energy in relativistic electrons radiating from frequency ν_1 to ν_2 with spectral index α [$S(\nu) \propto \nu^{\alpha}$] in a magnetic field B, giving flux density S_ν at frequency ν, is

$$E_{\rm e} = 4\pi \times 10^{12} \left(\frac{cz}{H_0}\right)^2 \left(1+\frac{z}{2}\right)^2 \frac{S_\nu}{\nu^\alpha} \frac{\nu_2^{0.5+\alpha} - \nu_1^{0.5+\alpha}}{\alpha + 0.5} B^{-3/2}$$

$$\approx aB^{-3/2}\,{\rm erg},$$

where the estimate $a = 3.6 \times 10^{48}$ corresponds to the radio data reported by Pedlar et al. (1990) at 332 MHz, and $H_0 = 75\,{\rm km\,s^{-1}\,Mpc^{-1}}$. It is also assumed that the particle energy distribution extends over the range responsible for the emission between $\nu_1 = 10$ MHz and $\nu_2 = 1.4$ GHz. These limits have been chosen to comprise the detected frequency interval.[1]

The total energy in particles and magnetic field is then

$$E_{\rm tot} = kE_{\rm e} + Vf\frac{B^2}{8\pi} = akB^{-3/2} + bfB^2,$$

where $b = 8.9 \times 10^{64}$, $V = 4\pi R^3/3$ is the volume, and $R = 2.7$ kpc (Pedlar et al. 1990). f represents the filling factor of the relativistic plasma, while the factor k accounts for the additional energy in relativistic particles accompanying the electrons that radiate above 10 MHz and any non-relativistic component, including turbulence ($k = 1$ for an electron–positron plasma emitting only in the above waveband; a typical value used in the literature is $k = 100$). This implies an equipartition magnetic field strength

$$B_{\rm eq} = 1.9 \times 10^{-5} \left(\frac{k}{f}\right)^{2/7}\,{\rm G},$$

and a corresponding equipartition pressure in particles and field of

$$P_{\rm p} + P_{\rm B} = \frac{ka}{3VfB^{3/2}} + \frac{B^2}{8\pi} \simeq 1.3 \times 10^{-2} \left(\frac{k}{f}\right)^{4/7}\,{\rm keV\,cm^{-3}}.$$

3.2 Pressure equilibrium between the relativistic and thermal plasmas

We now consider the relation between the pressure of the relativistic component and that of the X-ray-emitting gas. The thermal pressure in the rims immediately surrounding the lobes is $P_{\rm th} \approx 0.5\,{\rm keV\,cm^{-3}}$, and thus

$$\frac{P_{\rm th}}{P_{\rm p} + P_{\rm B}} \approx 40 \left(\frac{k}{f}\right)^{-4/7},$$

implying that in order to be in equilibrium at equipartition,

$$\frac{k}{f} \approx 6 \times 10^2.$$

This result can be interpreted in many ways. Perhaps k is large, indicating that the electron distribution extends to much lower energies than assumed by the fiducial synchrotron frequency of 10 MHz or the existence of heavy proton-rich jets. Alternatively, f may be small, and the radio plasma occupies only a tiny fraction of the apparent volume of the radio lobes. The plasma may be in sheets and filaments with a large covering fraction which have swept much of the cooler gas to the rims.

Finally, the radio plasma may not be in equipartition, as will indeed be shown in the next section. We plot in Fig. 6 the pressure against the magnetic field for various values of k/f. Pressure equilibrium between the thermal, magnetic and particle pressures and equipartition require a strong magnetic field and high value of k/f. From now on we do not assume that the plasma is in equipartition.

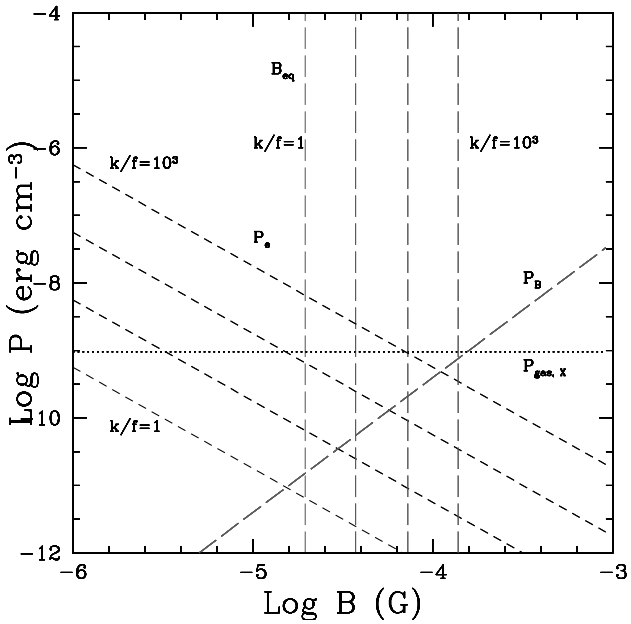

Figure 6. Pressure versus magnetic field for various values of k/f. The equipartition field and external gas pressure are also indicated.

[1] Given the crucial role of ν_1 we checked that our results are qualitatively consistent for ν_1 within at least the range 1–50 MHz.

3.3 Radiative and dynamical constraints

3.3.1 Radiative losses

We now consider further constraints that can be inferred from the spatial distribution of the radio emission at various frequencies, as well as dynamical constraints derived from the conditions of the X-ray-emitting gas. The only assumption we keep is that of equilibrium between the thermal and relativistic gas pressures, which constrains the relation between k/f and B such that

$$P_{\rm p} + P_{\rm B} = P_{\rm th}.$$

In the following we also consider constraints on the whole lobe, which is 7.5 kpc in radius (instead of the 2.7 kpc for region '3'), corresponding to an increase in volume by a factor of ∼21. The observed flux, and therefore particle energy, increases – using the maps of Pedlar et al. (1990) and assuming the same spectral index – by about a factor of 5.5 in going from the modelled 2.7 kpc radius region to the rest of the hole. The overall effect is to change the ratio k/f by less than a factor 2. We therefore plot only the allowed values of k/f in Fig. 7 for the whole lobe, as this region will be considered in the following.

Under the assumption of pressure equilibrium let us consider the radio emission. A limit on the maximum magnetic field is deduced by noting that GHz radio emission is seen throughout the N hole, so requiring that the synchrotron cooling time of the relativistic electrons there,

$$t_{\rm sync} = 4 \times 10^7 B_{-5}^{-3/2} \nu_9^{-1/2}\ {\rm yr},$$

be more than the age of the hole. A limit on this age is obtained by noting that the rims have not been shocked, so the hole has expanded at a velocity less than the sound speed $c_{\rm s}$ of the 3 keV gas in the rim; that is,

$$t_{\rm hole} > r/c_{\rm s} = 10^7\ {\rm yr},$$

where a radius of 7.5 kpc is used for the hole. This limits the magnetic field to $B < 2.5 \times 10^{-5}$ G, and consequently rules out any equipartition solution (see Fig. 6). Note that if the electrons diffuse between higher- and lower-field regions within the lobe then the limit is strengthened. Note also that the above condition implicitly assumes that no reacceleration of electrons occurs in the lobe. This is supported by the distribution of radio spectral index (see Fig. 4), which shows a smooth behaviour through the hole and a gradual steepening of the index from the inner to the outer parts (see also Section 4).

This constraint thus imposes a strong upper limit on B which is almost an order of magnitude below that required if $P_{\rm p} = P_{\rm B} = P_{\rm th}$. We conclude here that $P_{\rm p} = P_{\rm th} \gg P_{\rm B}$, and we obtain from Fig. 7 that $k/f < 500$.

If the field is very weak then cooling of relativistic electrons by synchrotron emission is reduced, and adiabatic and inverse Compton losses on the 3 K radiation field might be important. In particular the latter becomes more efficient than synchrotron emission for $B < 10^{-6}$ G.

3.3.2 Dynamical constraints

We finally examine constraints from the dynamics of the system. $P\,{\rm d}V$ work is of course done by the expanding bubble on the surrounding gas, with a power $\sim P_{\rm th} f V/t$. Most of this power will, however, propagate to large radii in the cluster as a sound wave (Fabian et al. 2000; Reynolds et al. 2001) and deposit little energy locally. In any case, the jet must be powerful enough to make the holes. In order to estimate such power we consider the evolution of an expanding bubble in a medium with constant pressure following Churazov et al. (2000). We modify their expressions for the expansion of the hole to include the effect of gas clumping (through the filling factor f).

To make a hole with the observed radius of 7.5 kpc requires

$$\frac{L_{45} t_7}{P_{\rm th} f} = 0.5,$$

when the expansion is already in the subsonic phase. We assume that the adiabatic index for the radio-emitting gas is 4/3, appropriate for a relativistic plasma, and parametrize the luminosity as $10^{45} L_{45}\ {\rm erg\ s^{-1}}$ and the age of the hole as $10^7 t_7$ yr. Secondly, the

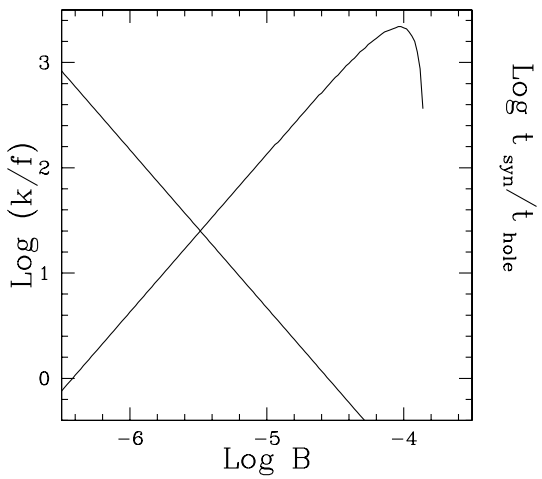

Figure 7. Ratio of k/f as a function of the magnetic field under the condition that the relativistic component is in pressure equilibrium with the thermal gas. The oblique line decreasing from left to right (labelled on the right-hand y-axis) indicates similar time-scales for the hole expansion and the relativistic electron cooling.

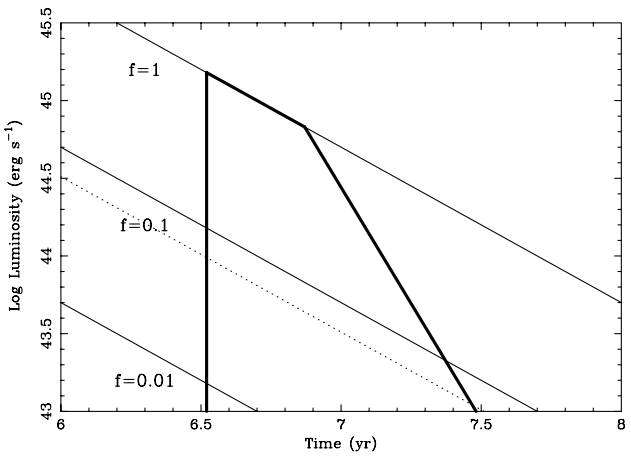

Figure 8. Dynamical constraints on the rate of power supplied to the N radio lobe. The three lines labelled with the filling factor f derive from the requirement to blow a hole equal in radius to that seen. To the left of the vertical line the hole expands at a velocity faster than the sound speed in the rims. To the right of the steeper diagonal line the bubble will rise faster than it expands, leading to it appearing detached from the centre, contrary to observations. The dotted line represents the minimum luminosity required to move gas to make the hole ($P_{\rm th} V/t$) for $f = 1$.

expansion rate must not be so fast as to shock the rim gas, which means that

$$\frac{L_{45}}{P_{\rm th} t_7^2 f} < 14.$$

In Fig. 7 the oblique solid line representing a decrease in k/f for increasing B corresponds to the condition that this expansion timescale is shorter than the synchrotron cooling one. Finally, the buoyancy of the hole must be considered (a detached low-density region will rise at close to the local virial velocity; Churazov et al. 2000), and the fact that it has not yet detached from the centre means (again modifying expressions from Churazov et al. 2000) that

$$L_{45} > 1.2 f^{5/2} t_7^2.$$

These three expressions define the allowable region in the power versus time plane, L, t, shown in Fig. 8.

Although it appears from Fig. 8 that very low powers are possible, work must be done in pushing the soft-X-ray-emitting gas out of the way to make the hole, even for low filling factors. The minimum luminosity required to move gas to make the hole is plausibly $P_{\rm th}V/t$, which is that needed to do work against gravity. This is shown as a dotted line in Fig. 8. Only if the soft-X-ray-emitting gas is removed by, say, mixing with hotter gas, requiring little power from the relativistic plasma, could this limit be overcome. We assume therefore that the filling factor of the lobes $f \leq 1$.

Further independent support for the possibility that the relativistic gas may be clumped (i.e. $f < 1$) comes from the requirement that relativistic electrons do not cool by Coulomb collisions in the thermal plasma. This would happen on time-scales $\sim 10^5$ yr if the two phases were significantly mixed. The magnetic field presumably provides the required confinement and insulation. Highly filamentary structures extending over extremely large linear scales have indeed been detected in radio observations (see the case of Fornax A, Fomalont et al. 1989). A similar situation can be envisaged for 3C 84. A direct estimate of the degree of clumping might be determined by the amount of inverse Compton-scattered radiation in the X-ray band, as this depends directly on the (relativistic) particle density. However, at the sensitivity level currently available, such a constraint only translates into $f^{2/3} B_5^{3/2} > 10^{-3}$.

The total power is high compared with the radiated luminosity in the radio band, which is of order 10^{40}–10^{41} erg s^{-1}. Most of the power either remains in the relativistic plasma in the lobes or is expended as $P\,{\rm d}V$ work on the surroundings. Unless there is an efficient method of dissipating that energy locally, it is likely to be transported by buoyancy and low-frequency sound waves to the outer parts of the cluster.

Fig. 8 gives us an upper limit on the dynamical age of the lobes which, through the comparison with the synchrotron cooling time in Fig. 7, translates into lower limits on both k/f and the magnetic field. Together with the constraint on f from Fig. 8 (i.e. from the need to make the hole) we now have fairly strong constraints on k (Fig. 9). It is restricted to be between 500 and 180, if $f = 1$.

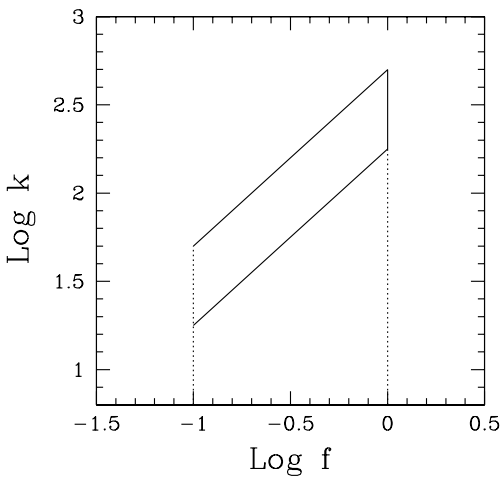

Figure 9. Joint constraints on k as a function of the filling factor f. Acceptable values lie within the oblique box.

4 THE OUTER LOBES

We now consider the information that can be inferred from the multifrequency radio maps of the outer holes.

4.1 The NW hole

The dynamical time of the outer NW hole, based again on buoyancy, is $\sim 6 \times 10^7$ yr if its filling factor by (low-density) radio plasma, f, is high.

A possible weak spur in the 330-MHz map reaches towards it, but it is one of several spurs. A radio spur clearly points to it only in the 74-MHz map. This is borne out by the steep spectral index (down to -1.7) seen on the S side of that spur (Fig. 4). The synchrotron cooling time of the radio spur is thus about $6 \times 10^7 B_{-5}^{-3/2}$ yr if we assume that a spectral ageing break occurs at about 100 MHz.

The good agreement between dynamical and synchrotron time-scales if $B_{-5} \approx 1$ indicates that the NW hole is consistent with the theory of its being an old detached radio lobe within which the magnetic field is in approximate pressure equilibrium with the surroundings. If this field $B \approx 10^{-5}$ G also pervades the N lobe, then $k/f \approx 100$.

Although the NW hole appears to be buoyant, suggesting that it is perhaps empty of thermal gas or at least has a high filling factor in relativistic plasma, a similar picture would emerge if the hole were filled with gas at the virial temperature ($\sim$7 keV) and f were small.

The edges of the NW hole appear sharp (Fig. 5). Presumably, large-scale magnetic fields along the surface provide the tension necessary to maintain the integrity of the hole against instabilities. It is possible too that magnetic fields in the thermal gas also restrict mixing, which might otherwise lead to fast cooling of the relativistic phase (note that very sharp boundaries between cooler and hotter gas have been seen in several clusters; e.g. Markevitch et al. 2000).

4.2 The S hole

The *Chandra* hole to the S is also at the end of a spur of 74-MHz emission. This time there is also a stronger spur at 330 MHz. The spectral index map shows a steep index in and to the W of this spur. It is again, presumably, another old radio lobe for which similar conclusions to those for the NW hole apply.

5 CONCLUSIONS

We have conducted a detailed physical analysis of 3C 84 in the Perseus cluster based on new observations of thermal X-ray and

non-thermal low-frequency radio emission. Our *Chandra* and 74-MHz radio images provide the highest-resolution view of the core of the Perseus cluster yet obtained in either X-rays or at low radio frequencies (<100 MHz), respectively. The requirements of pressure equilibrium between the relativistic plasma and the hot gas, and of the synchrotron cooling time-scale exceeding the dynamical one restrict the ratio $180 < k/f < 500$ in the inner N hole and exclude the possibility that the relativistic plasma and mean magnetic field are in equipartition. Further indications from the outer lobes support this result. $k \approx 340 \pm 160$ if $f \sim 1$, or, if the filling factor is less than unity, tends toward $k \approx 34 \pm 16$ when $f \sim 0.1$.

A value of $k \sim 340$ can be accounted for if the electron spectrum extends down to low energies corresponding to synchrotron emission at about 3 kHz. Otherwise, energetic protons must accompany the electrons.

The value of f greatly affects the estimate of the jet power: the dynamical constraints on the expansion and buoyancy of the hole require powers that greatly exceed (by up to a factor of 10^4) the minimum one, unless the filling factor is small. The most energetically efficient situation occurs when the filling factor is small. We estimate that $f > 0.1$ unless the holes are created in a non-energetic manner.

Much deeper observations with *Chandra* are required to clearly detect hotter gas in the holes and so constrain the filling factor of the relativistic plasma. Future, higher-resolution 74-MHz VLA observations would be useful for further delineating the structure of the low-frequency spurs. More desirable, even lower-frequency, observations must await the proposed Low Frequency Array (LOFAR).

ACKNOWLEDGMENTS

We thank Robert Schmidt for help with the X-ray data. Basic research in radio astronomy at the Naval Research Laboratory is supported by the Office of Naval Research. The National Radio Astronomy Observatory is operated by Associated Universities Inc., under cooperative agreement with the National Science Foundation. AC acknowledges the Italian MURST for financial support. ACF and KMB thank the Royal Society for support.

REFERENCES

Blundell K., Kassim N., Perley R., 1999, in Rao A. P., ed., Proc. IAU Coll. 199, The Universe at Low Radio Frequencies. Astron. Soc. Pac., San Francisco, in press (astro-ph/0004005)
Böhringer H., Voges W., Fabian A. C., Edge A. C., Neumann D. M., 1993, MNRAS, 264, L25
Churazov E., Forman W., Jones C., Böhringer H., 2000, A&A, 356, 788
Fabian A. C., Hu E. M., Cowie L. L., Grindlay J., 1981, ApJ, 248, 47
Fabian A. C. et al., 2000, MNRAS, 318, L65
Fomalont E. B., Ebneter K. A., van Breugel W. J. M., Ekers R. D., 1989, ApJ, 346, L17
Markevitch M. et al., 2000, ApJ, 541, 542
Pedlar A., Ghataure H. S., Davies R. D., Harrison B. A., Perley R., Crane P. C., Unger S. W., 1990, MNRAS, 246, 477
Reynolds C. S., Heinz S., Begelman M. C., 2001, ApJ, 549, L179
Schmidt R. W., Fabian A. C., Sanders J. S., 2002, MNRAS, submitted

This paper has been typeset from a TEX/LATEX file prepared by the author.